RSC Advances

PAPER

Cite this: *RSC Adv.*, 2016, **6**, 13548

Compromising high strength and ductility in nanoglass–metallic glass nanolaminates

Sara Adibi,[ab] Paulo S. Branicio*[a] and Roberto Ballarini[b]

Received 21st November 2015
Accepted 22nd January 2016

DOI: 10.1039/c5ra24715b

www.rsc.org/advances

We use large-scale molecular-dynamics simulations to investigate the deformation and failure mechanisms associated with tensile loading of 50 nm diameter $Cu_{64}Zr_{36}$ nanolaminate nanopillars constructed either as 5 nm thick layers of metallic glass (MG) or alternating 5 nm thick layers of MG and 5 nm grain sized nanoglass (NG). The MG–MG nanolaminate exhibits delayed shear band formation and diffused shear banding failure while the NG–MG nanolaminate shows exceptional plasticity to a strain of $\varepsilon = 0.15$ prior to a necking-type failure. The MG–MG nanopillar has approximately the same restricted ductility and ~15% lower strength than a reference MG nanopillar. The NG–MG nanopillar, on the other hand, retains the same level of ductility but displays ~20% higher strength than a reference NG nanopillar. These results suggest that nanolaminates of NG and MG offer promise for creating structures that combine outstanding strength and ductility.

1. Introduction

Eliminating the trade-off between strength and ductility is a long-standing goal in materials science and engineering. Methods that have been developed in the past decade to construct tailored microstructures offer promise towards greatly improving the performance of existing materials. Here we focus on constructing microstructures that could improve the strength and ductility of metallic glass components. In 1960 metallic glasses (MGs) were synthesized by fast quenching methods to increase the strength of conventional metals.[1] MGs possess distinctive properties compared to their conventional metallic crystalline counterparts, such as high strength and hardness, and the ability to store relatively high levels of elastic strain energy.[2–4] However, their low ductility limits their wide spread use.[5] Different strategies have been devised that have the potential to produce materials that will overcome this limitation. The use of composites and nanostructured MGs has been highlighted as the most promising approach. For example, the properties of MGs can be altered by the introduction of a high density of defects into their structure.[6,7] Such an example is the nanoglass (NG), which is generated by cold compression of glassy nanoparticles.[6,8–10] By introducing glass–glass interfaces with excess free volume and modified structure, NGs show enhanced ductility compared to corresponding MGs, but lower strength.[11–14] The continuous reduction in strength with respect to grain size is the result of the increased volume fraction of glass–glass interfaces. $Cu_{64}Zr_{36}$ bulk NG with a 5 nm average grain size retains only about 40% of the original MG strength while showing nearly homogeneous superplasticity. Developing methods to reduce the strength–ductility tradeoff of NGs is an important challenge. One approach is the creation of a composite made by mixing different compositions of MG or NG particles or NGs with different grain sizes.[15,16] Another approach is to create superstructures combining layers of MG and NG. Here we adopted the second strategy and investigate whether nanopillar-shaped nanolaminates constructed either as layers of MG or alternating layers of MG and NG can achieve combined high strength and high ductility.

2. Methodology

All nanopillars investigated have the composition $Cu_{64}Zr_{36}$. Nanolaminate nanopillars and reference MG and NG nanopillars are of cylindrical geometry with 50 nm diameter, aspect ratio 2.5, and contain approximately 16 million atoms. The interatomic forces are calculated using the embedded atom model potential developed by Cheng *et al.*[17] A time steps of 5 fs is employed in the integration of the equations of motion. Nanolaminate nanopillar models are constructed from previously generated MG and NG nanopillars. MG nanopillars models are generated from bulk metallic glass samples formed using a cooling rate of 10^{10} K s^{-1} from the liquid state, as described previously.[4,13,14] NG nanopillars are generated from the corresponding MG structure using the Poisson-Voronoi tessellation method.[18–20] MG and NG nanopillar models of identical dimensions are employed in the procedure used to generate the nanolaminate sample. Layers are filled with corresponding volume of material from either the original MG or

[a]*Institute of High Performance Computing, Agency for Science, Technology and Research, 1 Fusionopolis Way, 16-16 Connexis 138632, Singapore. E-mail: branicio@ihpc.a-star.edu.sg*

[b]*Department of Civil & Environmental Engineering, University of Houston, Houston, 77204, Texas, USA*

NG model. To produce a reference MG–MG nanolaminate sample, all atoms in the original periodic MG system are translated by applying a random shift to positions before each layer is filled. To avoid atomic overlapping at interfaces layers are filled until they reach a distance of 1 Å from the mathematically defined interfaces. In addition, after the nanolaminate model is produced, atoms are removed as necessary to ensure that no pair of atoms is closer than 2.2 Å. This step is motivated by the fact that in the CuZr bulk MG structure the average nearest neighbor distances are 2.7 Å for Cu–Cu, 3 Å for Cu–Zr, and 3.1 Å for Zr–Zr. Subsequently, the MG–MG and NG–MG nanolaminates are sintered by applying hydrostatic pressure of 3 GPa at a temperature of 50 K for 0.04 ns. This process ensure that the interfacial atomic structure is relaxed and porosity is minimized. The sintering is followed by relaxation of the system at zero pressure and 50 K for 0.04 ns. All samples are simulated under uniaxial tensile tests at the strain rate of 4×10^8 s^{-1}. Periodic boundary conditions are applied along the loading direction, and traction-free surfaces are used along the lateral directions. The temperature is maintained at 50 K throughout the loading. Engineering stress is calculated as the average atomic stress in the system based on the virial stress definition[21] and the use of the initial volume of the nanopillar model. The generation and evolution of local plastic deformation in the system is investigated by using the local atomic von Mises shear strain, η_{Mises}.[22] MD simulations are performed with LAMMPS[23] and visualizations with OVITO.[24]

3. Results and discussions

In order to characterize the strength and ductility of the MG–MG and NG–MG nanolaminates, simulations are first performed on reference nanopillars made from pure MG and NG. The nanopillars are illustrated in Fig. 1. For visualization purposes, layers and grains are displayed in different colors in order to highlight the nanostructures. We note that it has been reported that MGs undergo size dependent plasticity; smooth surface MG nanopillars with diameter less than 5 nm show extended plasticity and necking failure. However, smooth surface MG nanopillars with diameter of 50 nm are brittle and fail by shear band propagation with restricted plasticity.[25] Here, we explore the strength and ductility associated with MG–MG nanolaminates composed of 5 nm thick layers arranged along the cylinder axis. For the NG–MG nanolaminate, the NG layers have 5 nm average grain sizes. We note that previous studies revealed that bulk NGs undergo a transition from inhomogeneous deformation by single shear banding to homogeneous deformation and superplastic flow as grain sizes are reduced.[13,14] It has also been reported that NG nanopillars with 5 nm grain size exhibit necking failure and enhanced plasticity at the expense of their strength.[26] Nanopillars are simulated under tensile loading along their axes, *i.e.* perpendicular to the nanolaminate interfaces. In a previous investigation of MG–NG systems[27] tensile loading was applied parallel to the interfaces resulting in no apparent improvement in ductility and change in failure mode as compared to reference MG systems. As a required step to understand the general dependence of the strength and ductility of the nanolaminates on the direction of tensile loading the simulations here are performed using the other extreme case with the tensile loading applied perpendicular to the interfaces.

Either compressive or tensile loading may be used to evaluate the mechanical properties. However, to evaluate both strength and ductility it is critical to perform tensile loading testing in order to evaluate failure instabilities under complex stress such as shear banding, necking, *etc.* Therefore, we performed tensile loading simulations of all nanopillars. The tensile loading engineering stress–strain plots for the four nanopillars investigated are shown in Fig. 2. It is observed that the maximum stress (ultimate tensile strength) achieved by MG/NG/MG–MG/NG–MG nanopillars is 3.67/2.11/3.19/2.56 GPa, respectively. As expected both nanolaminates show strength values between the strength of the MG nanopillar and the NG

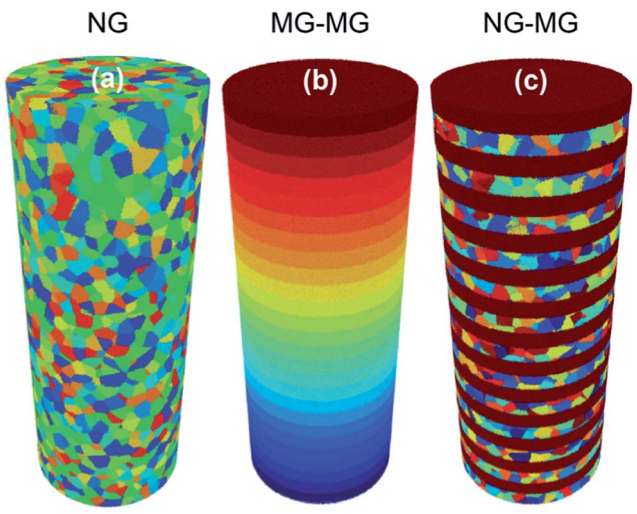

Fig. 1 Illustrations of the 50 nm diameter $Cu_{64}Zr_{36}$ metallic glass (MG) nanopillars used in the simulations. (a) Nanoglass (NG) with 5 nm grain size, (b) nanolaminate MG with 5 nm thick layers, (c) NG–MG nanolaminate with alternating 5 nm tick layers of MG and NG with 5 nm grain size. Grains and layers are shown in different colors to highlight the nanostructure.

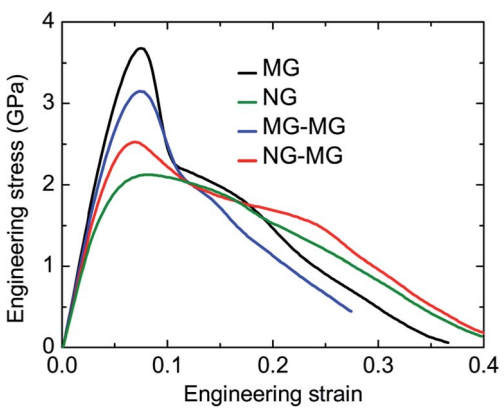

Fig. 2 Tensile loading engineering stress–strain curves for the MG, NG, nanolaminate MG, and nanolaminate NG–MG nanopillars.

nanopillar. The MG layers impart a significant strengthening to the reference NG pillar, as evidenced by the ~20% increase in strength (2.11 GPa to 2.56 GPa). Moreover, Fig. 2 shows that for both the MG and the MG–MG nanopillars there is a sharp stress drop immediately after the ultimate stress that results from the generation of a shear band. This contrasts with the gradual strain softening associated with the plasticity that develops in the NG–MG nanopillars. As expected, the introduction of the planar interfaces perpendicular to the loading direction lead to an ultimate stress of the MG–MG system, 3.19 GPa, ~15% lower than the 3.67 GPa strength of the MG nanopillar. The two systems, however, exhibit similar restricted ductility. The results clearly indicate that tailoring of NG–MG nanolaminates offer promise for achieving combined strength and ductility.

The atomic-level deformation mechanisms responsible for the stress–strain curves are examined through the distribution of atomic local shear strain. Regions with large atomic shear strain indicate high density of shear transformation zones (STZs).[28] Fig. 3 illustrates the deformation profile and the failure mechanism in all samples including the reference MG and NG structures. The contrast in deformation modes is sharp. The MG nanopillar, as shown in Fig. 3(a), develops well-defined deformation paths throughout its structure in the form of embryo shear bands. These embryos further develop into competing shear bands, which propagate across the system releasing elastic energy. Eventually a single shear band dominates the deformation profile and failure proceeds by propagation of this shear band throughout the nanopillar cross-section. On the other hand, Fig. 3(b) shows that the ductility and the ultimate failure of the 5 nm grain sized NG nanopillar is the result of necking. As discussed in detail previously[8,11–14,29–32] the NG design has a profound effect on the intrinsic failure mechanism of MGs. As can be seen in the frames of Fig. 3(b) the initial plastic deformation is distributed throughout the volume and follows the fine network of the softer glass/glass interfaces. At a strain of $\varepsilon \sim 0.25$, the deformation starts to localize and failure proceeds by generation of a well-defined necking.

A rather different scenario defines the deformation and failure of the nanolaminates, illustrated in Fig. 3(c) and (d). In Fig. 3(c) one can see the deformation profile for the nanolaminate nanopillar composed of layers of MG material. Interestingly, Fig. 3(c) shows that the onset of plastic deformation in the MG–MG pillar occurs predominantly along the interfaces of the MG layers. This result is intriguing.

The MG–MG glass–glass interfaces were characterize in detail in a previous investigations of NG.[14] It was demonstrated that these regions have excess free volume and distinguished structure when compared to that of MG. For the MG composition employed here, $Cu_{64}Zr_{36}$, glass–glass interfaces have ~1.1% excess free volume and a thickness of ~1.38 nm. The analysis of the Voronoi tessellation statistics indicates that structurally the interfaces are very similar to shear band regions. Therefore, MG–MG interfaces are relatively soft and weaker regions as compared to the MG layers. Consequently, the material at the interfaces reaches its elastic limit earlier than the material within the bulk of the MG layers. Therefore, it is reasonably expected that the MG–MG interfaces will accommodate the initial plastic deformation. On the other hand, the MG–MG interfaces in this work are designed to be perpendicular to the strain loading direction. It is expect that such design will prevent premature plasticity *i.e.* sliding of MG layers against each other, since the Schmid factor, and as a consequence the resolved shear stress along the interfaces, will be zero.[33] Nonetheless, one can clearly observe that significant plastic deformation do take place at the MG–MG interfaces creating a peculiar profile of deformation. It should be noted that the initial constrained plastic deformation at the MG–MG interfaces delay the build up of stress in the system and extend the deformation that the nanopillar can withstand

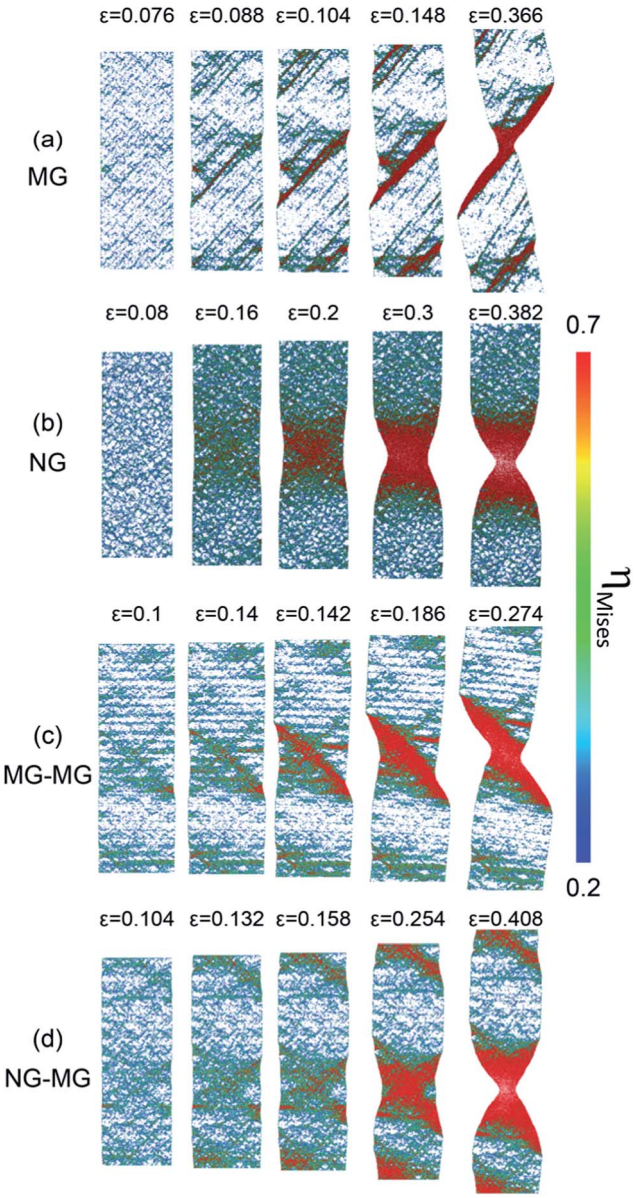

Fig. 3 Illustrations of the deformation and failure of (a) MG, (b) NG, (c) nanolaminate MG, and (d) nanolaminate NG–MG nanopillars. The color indicates the von Mises local atomic shear strain, η_{Mises}. For clarity, only atoms with η_{Mises} > 0.2 are shown. Illustrations are produced from visualizations of a 1 nm thick slice along the nanopillars cutting their cross section.

before failure by shear band propagation. Even though similar to the failure of the MG nanopillar, the MG–MG nanolaminate shows a relatively broad strain localization region. Although shear off set is clearly seen the dominant shear band is diffused and significantly thicker than the corresponding band in the MG pillar. Therefore, from the profiles of deformation in Fig. 3(a) and (c) one can see that the deformation of MG and MG–MG nanopillars bear similarities and differences. While both ultimately fail by propagation of a dominant shear band the latter shows enhanced plasticity rooted at the interfaces. That creates the horizontal pattern of deformation seen in the first panel of Fig. 3(c). In contrast, the first panel of Fig. 3(a) shows a ~45-degree pattern, characteristic of the generation of precursor shear bands.

The deformation and failure of the NG–MG nanopillar is illustrated in Fig. 3(d) and highlight the mechanism responsible for its good combination of strength and ductility. As expected, due to the presence of highly ductile NG layers, the initial plastic deformation of these structures is spread throughout the volume. One can see the effects of the NG design manifesting strongly in the deformation of the NG–MG nanopillars. The enhancement of the ductility induced solely by the presence of interfaces, as noted in the MG–MG nanopillar, is also active in the NG–MG though it is rather mild compared to the homogenization of the deformation caused by the presence of the highly ductile NG layers. At the extended deformation of $\varepsilon = 0.158$ strain localization starts to build up in the system though in a significantly more homogeneous mode than in the MG–MG nanolaminate nanopillars. One can see the formation of necking in two spots along the NG–MG nanopillar. Eventually, the necking at one of the regions dominate the deformation profile and the failure occurs by the development of a well-defined necking region that fails at strain in excess to $\varepsilon = 0.4$, indicating an outstanding plastic deformation of the NG–MG nanolaminate nanopillar.

Additional insights into the plastic deformation of the nanopillars are provided by the fraction of the atoms with large shear strain. That information provides insights into the onset and development of plastic deformations and indicates the volume of each nanopillar, which is contributing to the observed plastic deformation. Here the fraction of atoms with large atomic shear strain is calculated based on the von Mises shear strain assuming a threshold of $\eta_{\text{Mises}} = 0.2$, following previous investigations.[13,14] Based on Fig. 2 and 3 the results shown in Fig. 4 indicates that the fraction of atoms involved in plastic deformation for all nanopillars rises steadily at the yield point, slightly earlier for the nanolaminates and NG nanopillars. The fractions reach a steady value at the point where either a shear band propagates through the nanopillar cross section, in the case of MG and MG–MG nanopillars, or necking starts to develop, in the case of NG and NG–MG nanopillars. Two important insights can be extracted from the curves of Fig. 4. First, the MG–MG nanolaminate design enhances to a limited degree the fraction of atoms involved in plastic deformation compared to the pure MG case. This result is directly related to the presence of glass–glass interfaces in this design. Second, the fraction of atoms involved in plasticity in the NG–MG nanolaminate is about double that of the MG or MG–MG nanolaminate, implying an exceptional enhancement of plasticity caused by the introduction of NG layers in the nanolaminates. That illustrates the plastic deformation in the NG–MG is effectively delocalized and similar to that experienced by the exceptionally plastic NG nanopillars. One should note that the fraction of atoms involved in the deformation is very particular to the system simulated and depends directly on several factors such as the system size, aspect ratio, and strain-rate applied. Nonetheless, the sharp contrast between the mechanical properties of the NG–MG nanolaminate nanopillar and that of the MG nanopillar is expected to be independent of such factors.

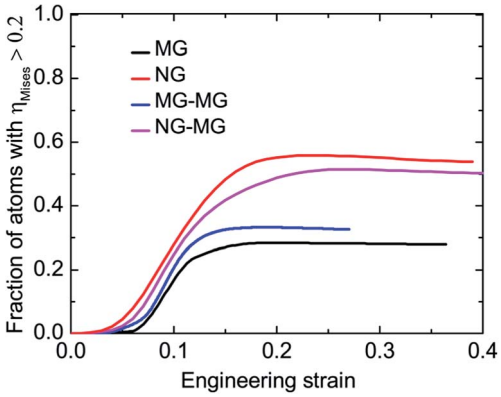

Fig. 4 Analysis of atomic deformation engagement in MG and NG reference nanopillars as well as MG–MG and NG–MG nanolaminate nanopillars based on the fraction of atoms with $\eta_{\text{Mises}} > 0.2$ during deformation.

The data shown in Fig. 4 can be used to further quantify the plastic deformation and enhancement of ductility in the NG–MG nanolaminate nanopillar. It is not trivial to pinpoint the exact location of the yield point given thermal fluctuations and the effect of the high strain rate utilized. Nonetheless, assuming that the fraction of atoms with large shear strain at 1% indicates unambiguously the yield point we can use Fig. 4 to estimate the yield strain. From the data in Fig. 4 the yield strain is estimated for MG/NG/MG–MG/NG–MG at $\varepsilon = 0.062/0.031/0.046/0.039$. Based on that the yield stress estimated from the data shown in Fig. 2 for MG/NG/MG–MG/NG–MG is 3.46/1.42/2.51/1.95 GPa. The rise of localization and failure of the nanopillars, either by shear banding or necking, can also be estimated from Fig. 4. Taking the maximum of each curve as a failure point, where no additional local plastic deformation occurs in the nanopillars, indicates a fracture strain for MG/NG/MG–MG/NG–MG at $\varepsilon = 0.18/0.23/0.19/0.26$. We define ductility in the context of this work as both the ability to fail by necking and the ability to generate and develop inelastic deformation (plasticity) until failure, either by shear banding or necking. It is clear from Fig. 3 that both the NG and NG–MG nanopillars are effective at constraining the propagation of shear bands and fail by necking. From the values of yield strain and fracture strain mentioned previously we can estimate the total plastic strain for MG/NG/MG–MG/NG–MG to be $\varepsilon = 0.118/0.199/0.144/0.221$. Therefore,

using both definitions the NG–MG nanolaminate nanopillar presents a significant enhancement of ductility.

It is instructive to compare the predictions of this work with closely related investigations of metallic glasses and nanoglasses. In a recent work Sha *et al.*[27] investigated the mechanical properties of a CuZr metallic glass coated with a CuZr 5 nm grain size nanoglass layer. Since shear bands often are nucleated at the surfaces of metallic glasses, the results of this study showed delay shear band formation and accommodation of the initial overall deformation as plastic events in the nanoglass coating layer. Nonetheless, the coated metallic glass systems fail by propagation of a dominant shear band with limited increased in overall ductility. However, the results are important and suggest that nanoglass coating maybe used effectively to increase surface flaw tolerance in bulk metallic glasses. Using a different approach Sha *et al.*[16] investigated the strength and ductility of a CuZr bimodal grain sized nanoglass. They created composite NGs by combining nanoglass grains of 5 nm and 15 nm at different proportions. From previous work on CuZr NG[13,14] it is known that NGs with 5 nm grain size are superplastic while significantly weaker than the MG counterpart. On the other hand NG with 15 nm grain size preserve most of the strength of the MG while still presenting limited increased in plasticity and still failing by shear banding. The results showed that at a suitable fraction combination the bimodal grain sized NGs is able to increase strength by ~10% compared to that of the 5 nm NG architecture while still preserving the superplasticity. The results of our work resonate with the conclusions of the two previously discussed investigations. In order to take full advantage of the superior ductility of small grain size NG it should be used in carefully designed architectures *e.g.*, as a coating to impart surface flaw tolerance, in a bimodal grain size NG to impart high ductility to a large and strong grain size NG, or by making nanolaminates with MG to improve significantly the strength while preserving the ductility of the NG.

The idea of using nanolaminates of a metallic glass with ductile materials, such as crystalline metals, to obtain a strong and ductile combined material has been explored recently.[34–38] Wang *et al.*[34,35] fabricated Cu–CuZr nanolaminates with ~5–10 nm CuZr amorphous layers intercalated with ~35 nm crystalline Cu layers. Tensile loading tests revealed that the nanolaminates have exceptional ductility, with no necking, and an elongation to failure of 14%, which is much higher than that observed in crystalline–crystalline nanolaminates, typically <2%. Atomistic simulations showed that the thin CuZr amorphous layer in the nanolaminates no longer develop shear bands and that it serves as an effective sink for dislocations produced in the Cu crystalline thicker layers. Interestingly, the amorphous–crystal interfaces are also identified as sources for dislocation nucleation and emission. Kim *et al.*[36,37] evaluated the mechanical response of nanolaminates with alternating thicker layers of amorphous CuZr with ~112 nm and thinner layers of crystalline Cu with ~16 nm. The results show strength of 2.5 GPa, 25% better than for pure amorphous CuZr. Catastrophic failure typical of metallic glasses was suppressed and samples failed with a strain of 4%. In a closely related investigation Guo *et al.*[38] performed nanoindentation on Cu–CuZr nanolaminates with Cu layers of 10 nm and CuZr layers of 100 nm and the results suggest that the deformation proceeds by coupling of dislocations in the crystalline layer to shear bands in the amorphous layer. This coupling induces displacement of crystalline clusters into the amorphous layers leading to an intense chemical mixing in a 2–3 nm layer at the interface generating an effective amorphous–crystalline nanocomposite.

The results of our work show that the non-dislocation based plasticity induced in a NG layer is delocalized and spread along the whole NG laminate volume. Therefore, in sharp contrast with the Cu–CuZr nanolaminates, the NG ductile layer does not actively promote the generation and propagation of shear bands in the MG layers of the NG–MG nanolaminate. On the other hand, if eventual shear bands generated in the MG layers propagate and reach the NG–MG interface, they are not expected to generate further localized plastic deformations in the NG layer, in contrast with the predicted dislocation propagation in the crystalline Cu layer in the Cu–CuZr nanolaminates. Hence, the overall ductility in the NG–MG nanolaminates is expected to be superior to that presented in the Cu–CuZr nanolaminates, since the former is able to promote delocalization of the plastic deformation more effectively. In addition, the link of local plastic events in the crystalline Cu layer, dislocations, and amorphous CuZr layer, shear bands, is nonexistent in the NG–MG nanolaminates.

As a final note, it should be highlighted that this work is a proof of concept and is not intended to prescribe an optimal combination to construct a nanolaminate structure to optimize strength and ductility. While the results show a significant improvement in strength from the 5 nm grain size NG of about 20% that should not be considered a limit. Future works should evaluate the effects of grain size, NG layer thickness, and the distance between NG layers. It should be noted that another important phenomena observed for small grain size NG and constrained MG systems is completely neglected here, *i.e.* strain hardening. In a previous investigation by Adibi *et al.*[26] it was highlighted that 3 nm grain sized CuZr NG exhibit strain hardening until failure by necking occurs. Tensile loading experiments[39] and simulations[40] of deeply notched MG samples also show evidence of densification and strain hardening. It is therefore expected that carefully designed NG–MG nanolaminates can be built to capitalize on the strain hardening of the NG layer in order to optimize the overall plasticity and strength of the nanolaminate architecture.

4. Conclusions

We performed MD simulations to characterize the deformation and failure mechanisms of $Cu_{64}Zr_{36}$ MG–MG and NG–MG nanolaminates, and have shown that structural heterogeneity is an effective strategy to tailor the mechanical properties of metallic glasses and achieve combined exceptional strength and ductility. By using nanolaminates the failure transitions from the propagation of a discrete shear band to a distributed plastic-type behavior (that one can consider embryo-sized nanoshear bands) that ultimately produces necking. The results presented here can be considered a computational-based proof

of concept that by alternating layers of MG and NG one can construct nanopillars whose strength is significantly higher than homogeneous NG structures while retaining their high ductility. Future studies are required to determine the effects of the diameter and aspect ratio on strength and ductility of the pillars. In addition, it is also important to characterize the possible interaction between glass–glass interfaces and how the ductility of the nanolaminates depends on the thickness of the layers for both MG–MG and NG–MG cases.

Acknowledgements

S. A. acknowledges financial support from A*STAR through the SINGA Award. This work was partially supported by the A*STAR Computational Resource Centre through the use of its high performance computing facilities.

Notes and references

1 W. Klement, R. H. Willens and P. Duwez, *Nature*, 1960, **187**, 869–870.
2 A. L. Greer, *Science*, 1995, **267**, 1947–1953.
3 A. Inoue and A. Takeuchi, *Mater. Trans.*, 2002, **43**, 1892–1906.
4 P. Thamburaja, B. Klusemann, S. Adibi and S. Bargmann, *Appl. Phys. Lett.*, 2015, **106**, 051903.
5 A. S. Argon, *Acta Metall.*, 1979, **27**, 47–58.
6 H. Gleiter, *Acta Mater.*, 2008, **56**, 5875–5893.
7 R. A. Andrievski, *Phys.–Usp.*, 2013, **56**, 261–268.
8 X. L. Wang, F. Jiang, H. Hahn, J. Li, H. Gleiter, J. Sun and J. X. Fang, *Scr. Mater.*, 2015, **98**, 40–43.
9 M. Ghafari, S. Kohara, H. Hahn, H. Gleiter, T. Feng, R. Witte and S. Kamali, *Appl. Phys. Lett.*, 2012, **100**, 133111.
10 H. Gleiter, T. Schimmel and H. Hahn, *Nano Today*, 2014, **9**, 17–68.
11 Y. Ritter, D. Şopu, H. Gleiter and K. Albe, *Acta Mater.*, 2011, **59**, 6588–6593.
12 K. Albe, Y. Ritter and D. Şopu, *Mech. Mater.*, 2013, **67**, 94–103.
13 S. Adibi, Z. D. Sha, P. S. Branicio, S. P. Joshi, Z. S. Liu and Y. W. Zhang, *Appl. Phys. Lett.*, 2013, **103**, 211905.
14 S. Adibi, P. S. Branicio, Y. Zhang and S. P. Joshi, *J. Appl. Phys.*, 2014, **116**, 043522.
15 H. Gleiter, *Beilstein J. Nanotechnol.*, 2013, **4**, 517–533.
16 Z. D. Sha, P. S. Branicio, Q. X. Pei, Z. S. Liu, H. P. Lee, T. E. Tay and T. J. Wang, *Nanoscale*, 2015, **7**, 17404–17409.
17 Y. Q. Cheng, A. J. Cao, H. W. Sheng and E. Ma, *Acta Mater.*, 2008, **56**, 5263–5275.
18 J. L. Finney, *J. Comput. Phys.*, 1979, **32**, 137–143.
19 W. Brostow, J.-P. Dussault and B. L. Fox, *J. Comput. Phys.*, 1978, **29**, 81–92.
20 M. Tanemura, T. Ogawa and N. Ogita, *J. Comput. Phys.*, 1983, **51**, 191–207.
21 P. S. Branicio and D. J. Srolovitz, *J. Comput. Phys.*, 2009, **228**, 8467–8479.
22 F. Shimizu, S. Ogata and J. Li, *Mater. Trans.*, 2007, **48**, 2923–2927.
23 S. Plimpton, *J. Comput. Phys.*, 1995, **117**, 1–19.
24 A. Stukowski, *Modell. Simul. Mater. Sci. Eng.*, 2010, **18**, 015012.
25 S. Adibi, P. S. Branicio, R. Liontas, D. Z. Chen, J. R. Greer, D. J. Srolovitz and S. P. Joshi, *Extreme Mechanics Letters*, 2015, **5**, 88–95.
26 S. Adibi, P. S. Branicio and S. P. Joshi, *Sci. Rep.*, 2015, **5**, 15611.
27 Z. D. Sha, L. C. He, Q. X. Pei, Z. S. Liu, Y. W. Zhang and T. J. Wang, *Scr. Mater.*, 2014, **83**, 37–40.
28 A. J. Cao, Y. Q. Cheng and E. Ma, *Acta Mater.*, 2009, **57**, 5146–5155.
29 H. Gleiter, T. Schimmel and H. Hahn, *Nano Today*, 2014, **9**, 17–68.
30 J. X. Fang, U. Vainio, W. Puff, R. Würschum, X. L. Wang, D. Wang, M. Ghafari, F. Jiang, J. Sun, H. Hahn and H. Gleiter, *Nano Lett.*, 2012, **12**, 5058.
31 D. Şopu, K. Albe, Y. Ritter and H. Gleiter, *Appl. Phys. Lett.*, 2009, **94**, 191911.
32 D. Şopu, Y. Ritter, H. Gleiter and K. Albe, *Phys. Rev. B: Condens. Matter Mater. Phys.*, 2011, **83**, 100202.
33 Z. D. Sha, P. S. Branicio, V. Sorkin, Q. X. Pei and Y. W. Zhang, *Diamond Relat. Mater.*, 2011, **20**, 1303–1309.
34 Y. Wang, J. Li, A. V Hamza and T. W. Barbee, *Proc. Natl. Acad. Sci. U. S. A.*, 2007, **104**, 11155–11160.
35 Y. M. Wang, A. V. Hamza and T. W. Barbee, *Appl. Phys. Lett.*, 2007, **91**, 061924.
36 J.-Y. Kim, X. Gu, M. Wraith, J. T. Uhl, K. A. Dahmen and J. R. Greer, *Adv. Funct. Mater.*, 2012, **22**, 1972–1980.
37 J.-Y. Kim, D. Jang and J. R. Greer, *Adv. Funct. Mater.*, 2011, **21**, 4550–4554.
38 W. Guo, E. A. Jägle, P.-P. Choi, J. Yao, A. Kostka, J. M. Schneider and D. Raabe, *Phys. Rev. Lett.*, 2014, **113**, 035501.
39 Z. T. Wang, J. Pan, Y. Li and C. a. Schuh, *Phys. Rev. Lett.*, 2013, **111**, 1–5.
40 Z. D. Sha, Q. X. Pei, Z. S. Liu, Y. W. Zhang and T. J. Wang, *Sci. Rep.*, 2015, **5**, 10797.